RAA 2016 Vol. **16** No. **3**, 44 (8pp) doi: 10.1088/1674–4527/16/3/044
http://www.raa-journal.org *http://iopscience.iop.org/raa*

***R**esearch in*
***A**stronomy and*
***A**strophysics*

The age of the halo as determined from halo field stars

Jin-Cheng Guo[1,2], Chao Liu[1] and Ji-Feng Liu[1,2]

[1] Key Laboratory of Optical Astronomy, National Astronomical Observatories, Chinese Academy of Sciences, Beijing 100012, China; *jcguo@nao.cas.cn*
[2] College of Astronomy and Space Sciences, University of Chinese Academy of Sciences, Beijing 100049, China

Received 2015 May 12; accepted 2015 October 16

Abstract The age of the Galactic halo is a critical parameter that can constrain the origin of the stellar halo. In general, the Galactic stellar halo is believed to be very old. However, different independent measurements and techniques based on various types of stars are required so that the age estimates of the Galactic halo are accurate, robust, and reliable. In this work, we provide a novel approach to determine the age of the halo with turn-off stars. We first carefully select 63 field halo turn-off stars from the literature. Then, we compare them with the GARSTEC model, which takes the process of atomic diffusion into account in the $B-V$ vs. metallicity plane. Finally, we run Monte Carlo simulations to consider the uncertainty of the color index and obtain the age of 10.5 ± 1.5 Gyr. This result is in agreement with previous studies. Future works are needed to collect more turn-off samples with more accurate photometry to reduce the uncertainty of the age.

Key words: galaxies: halos — Galaxy: evolution — stars: kinematics and dynamics

1 INTRODUCTION

The Milky Way is surrounded by a stellar halo, whose origin is still not very clear. Two famous hypotheses about the formation of the halo have been established. Eggen et al. (1962) claimed that the Galactic halo was formed from a rapid monolithic collapse, while Searle & Zinn (1978) declared that it was formed via accretion of nearby satellite galaxies over several Gyr. Recently, Carollo et al. (2007) argued that the halo is composed of two broadly overlapping structures: the inner and the outer halo. These two components show distinct density profiles, stellar orbits, and metallicities. The inner halo dominates the radii only up to 10–15 kpc, while the outer halo is located beyond (de Jong et al. 2010). However, this dichotomy scenario is challenged by Schönrich et al. (2011, 2014), who suggest that it is not true due to systematic bias in distance estimation. This debate makes it very important that other parameters, e.g. age, may play a critical role to constrain the structure and origin of the stellar halo.

Although it is quite difficult to determine the age of a star, several approaches have been well studied to measure the age of the stellar halo as a whole. First, globular clusters can be used as tracers to probe the age of the halo. In general, the approaches using globular clusters compare the observed color-magnitude diagram with the theoretical stellar models or isochrones, assuming that the globular clusters are simple stellar populations (Searle & Zinn 1978; Chaboyer et al. 1996; Sarajedini 1997). Second, the relatively more accurate ages can be determined using the difference in the color between the main sequence turn-off and the base of the red giant branch (Sarajedini & Demarque 1990; Vandenberg et al. 1990). Third, other techniques for the ages of halo stars include measurement of the abundances of radioactive species, e.g. thorium and uranium (Frebel et al. 2007). However, the precision of this method cannot be better than about 2 to 3 billion years, due to limitations related to the difficulty in measuring the weak signatures of these elements in stellar spectra, and incomplete knowledge about the production ratios of such species in nuclear reactions that involve rapid neutron capture. Recently, Kalirai (2012) employed a new technique to determine the age of the halo via the masses of halo stars that have just turned into white dwarfs. The relationship between the mass and the age was calibrated by comparing them with newly formed white dwarfs in globular cluster Messier 4, which is estimated to have an age of 12.5 ± 0.5 Gyr (Dotter et al. 2010). Finally, the author obtained that the age of the inner halo is 11.4 ± 0.7 Gyr.

Finally, theoretical predictions on the relationship between the age, temperature, composition, distance, and luminosity can place a given star at a unique position in an observed two dimensional diagram of color versus apparent brightness. This can yield the age of the halo as well (Holmberg et al. 2009). Jofré & Weiss (2011) used a similar technique to determine the age using the temperature for the main sequence turn-off sample of SDSS DR7 halo stars identified by using metallicity. They obtained that the age of the halo is 10–12 Gyr, which agrees with the absolute age of the old globular clusters in the inner halo.

In this paper we determine the age of the Galactic halo with field halo main sequence turn-off stars selected from the Set of Identifications, Measurements, and Bibliography for Astronomical Data (SIMBAD) archive. Unlike Jofré & Weiss (2011), the halo membership is determined via a kinematic method rather than metallicity. The color-metallicity diagram of the turn-off stars is then used to determine the age. In Section 2, we describe how we choose the sample from SIMBAD, how to calculate the three-dimensional (3-D) velocity, and how to discriminate the halo stars from the phase space. The field halo stars from our sample are then mapped onto an H-R diagram with a stellar evolution model so that the turn-off stars can be identified. In Section 3, we develop the approach to determine the age of the halo using the selected turn-off stars. We discuss some issues that may affect the accuracy of the determination and finally draw a brief conclusion in Section 4.

2 DATA

2.1 Data Selection from Databases

We select a sample from the SIMBAD database (Wenger et al. 2000). As of 2014 Dec 3, SIMBAD contains information about 7 615 021 objects under 18 997 314 different names, with 298 024 bibliographical references and 11 031 086 bibliographic citations. First, we select stars within a distance of 1 kpc, which is equivalent to having a parallax of at least 1 mas.

Among them, 36 824 stars with available radial velocity are selected. After excluding those stars with no proper motion, metallicity, or apparent magnitude B and V, or their parallax errors are larger than 100%, 36 219 stars are left in the end. It is noted that the parallaxes and their errors from SIMBAD are all from the *Hipparcos* catalogue (Perryman et al. 1997), so they are self consistent. However, other parameters, e.g., proper motions, metallicities, radial velocities, and magnitudes are compiled from different references and hence may not be self consistent with each other. Although this may introduce additional uncertainty or systematic bias into our final result, it is so far the best sample suitable for the estimation of the age of the halo we can find from the literature. *Gaia* (Perryman et al. 2001) will provide a larger self consistent sample with parallaxes, proper motions, radial velocities, and stellar atmospheric parameters to higher accuracies, which would be better data that can improve this work in the future.

2.2 Kinematic Identification of the Halo Stars

2.2.1 Stellar kinematics

In order to obtain the field halo stars from the 36 219 stars in this sample, we first calculate the 3-D heliocentric velocities for these stars from their positions, parallaxes, proper motions, and radial velocities. Then we move them to the frame with respect to the local standard of rest (LSR) so that the effect of solar motion can be removed.

Table 1 Characteristic velocity dispersions of the thin disk, thick disk and halo. X is the observed fraction of the population in the solar neighborhood. Velocity units are km s^{-1} (Bensby et al. 2003).

	X	σ_U	σ_V	σ_W	$V_{\rm asym}$
Thin disk	0.94	35	20	16	−15
Thick disk	0.06	67	38	35	−46
Halo	0.0015	160	90	90	−220

First, the 3-D heliocentric velocity U, V and W of a star can be derived from Johnson & Soderblom (1987).

$$\begin{bmatrix} U \\ V \\ W \end{bmatrix} = \mathbf{B} \cdot \begin{bmatrix} \rho \\ k\mu_\alpha/\pi \\ k\mu_\delta/\pi \end{bmatrix} = \mathbf{T} \cdot \mathbf{A} \cdot \begin{bmatrix} \rho \\ k\mu_\alpha/\pi \\ k\mu_\delta/\pi \end{bmatrix} , \quad (1)$$

where $k = 4.74057$ km s^{-1} yr, π is the parallax in arcsec, ρ is the radial velocity in km s^{-1}, and μ_α and μ_δ are the proper motions in right ascension and declination, respectively, in arcsec yr^{-1}. The transformation matrices on the right-hand side of Equation (1) are written as

$$\begin{aligned} \mathbf{T} = & \begin{bmatrix} +\cos\theta_0 & +\sin\theta_0 & 0 \\ +\sin\theta_0 & -\cos\theta_0 & 0 \\ 0 & 0 & +1 \end{bmatrix} \\ & \begin{bmatrix} -\sin\delta_{\rm NGP} & 0 & +\cos\delta_{\rm NGP} \\ 0 & -1 & 0 \\ +\cos\delta_{\rm NGP} & 0 & +\sin\delta_{\rm NGP} \end{bmatrix} \\ & \begin{bmatrix} +\cos\alpha_{\rm NGP} & +\sin\alpha_{\rm NGP} & 0 \\ +\sin\alpha_{\rm NGP} & -\cos\alpha_{\rm NGP} & 0 \\ 0 & 0 & +1 \end{bmatrix} , \end{aligned} \quad (2)$$

and

$$\begin{aligned} \mathbf{A} &= \begin{bmatrix} +\cos\alpha\cos\delta & -\sin\alpha & -\cos\alpha\sin\delta \\ +\sin\alpha\cos\delta & +\cos\alpha & -\sin\alpha\sin\delta \\ +\sin\delta & 0 & +\cos\delta \end{bmatrix} \\ &= \begin{bmatrix} \cos\alpha & \sin\alpha & 0 \\ \sin\alpha & -\cos\alpha & 0 \\ 0 & 0 & -1 \end{bmatrix} \begin{bmatrix} \cos\delta & 0 & -\sin\delta \\ 0 & -1 & 0 \\ -\sin\delta & 0 & -\cos\delta \end{bmatrix} . \end{aligned} \quad (3)$$

The uncertainties in U, V, and W can be propagated from

$$\begin{aligned} \begin{bmatrix} \sigma_U^2 \\ \sigma_V^2 \\ \sigma_W^2 \end{bmatrix} = \mathbf{C} \cdot & \begin{bmatrix} \sigma_\rho^2 \\ (k/\pi)^2[\sigma_{\mu_\alpha}^2 + (\mu_\alpha\sigma_\pi/\pi)^2] \\ (k/\pi)^2[\sigma_{\mu_\delta}^2 + (\mu_\delta\sigma_\pi/\pi)^2] \end{bmatrix} \\ & + 2\mu_\alpha\mu_\delta k^2\sigma_\pi^2/\pi^4 \begin{bmatrix} b_{12}\cdot b_{13} \\ b_{22}\cdot b_{23} \\ b_{32}\cdot b_{33} \end{bmatrix} , \end{aligned} \quad (4)$$

where the elements in the matrix $\mathbf{C}$ are the squares of the corresponding elements in $\mathbf{B}$; σ_ρ, σ_π, σ_{μ_α}, and σ_{μ_δ} are uncertainties in the radial velocity, parallax, and proper motions in right ascension and declination, respectively. $\alpha_{\rm NGP} = 192.25^\circ$ and $\delta_{\rm NGP} = 27.4^\circ$. Then the velocities derived above need to be shifted from the coordinates with respect to the Sun to the ones with respect to the LSR. Here we adopt the solar motion of ($U_\odot$, $V_\odot$,

$W_\odot) = (+11.1, +12.24, +7.25)$ km s^{-1} with respect to the LSR (Schönrich et al. 2010).

For each star, its ($U_{\rm LSR}$, $V_{\rm LSR}$, $W_{\rm LSR}$) is used to separate whether it belongs to the thin disk, thick disk or halo.

2.2.2 *Probability of being a halo star*

The probability of belonging to the halo, thick disk or thin disk for a star is calculated assuming that the velocities ($U_{\rm LSR}$, $V_{\rm LSR}$, $W_{\rm LSR}$) follow a 3-D Gaussian distribution:

$$\mathrm{Prob} = c \cdot \exp\Big(-\frac{U_{\rm LSR}^2}{2\sigma_U^2} - \frac{(V_{\rm LSR} - V_{\rm asym})^2}{2\sigma_V^2} - \frac{W_{\rm LSR}^2}{2\sigma_W^2}\Big), \quad (5)$$

where $c = (2\pi)^{-3/2}(\sigma_U\sigma_V\sigma_W)^{-1}$ normalizes the expression. σ_U, σ_V and σ_W are the velocity dispersions in three dimensions and $V_{\rm asym}$ is the asymmetric drift, which varies with different components and is listed in Table 1.

We define the probability ratio of belonging to the halo as

$$f_{\rm halo} = \frac{\mathrm{Prob_{halo}}}{\mathrm{Prob_{halo}} + \mathrm{Prob_{thin}} + \mathrm{Prob_{thick}}}. \quad (6)$$

We classify a star as being a good candidate halo star when this ratio is larger than 80% and one to be a possible halo star when it is larger than 60%. This classification criterion is verified in the Toomre diagram shown in Figure 1. It shows that good candidate halo stars (green crosses) are non-rotating or even have retrograde rotation with higher kinetic energy in their U and W components, while the possible halo stars (blue crosses) have moderate rotation. The thick and thin disk stars (red and black symbols, respectively) have stronger rotation with smaller velocity dispersion.

2.3 The Halo turn-off Stars as the Age Indicators

In principle, the age of the halo can be determined from the position of the turn-off halo stars in the H-R diagram. Therefore, we first select the halo turn-off stars and correct for interstellar extinction in $B-V$ to move them back to their intrinsic colors. Then, we can compare the turn-off position with theoretical isochrones to determine the age of the halo.

In order to select turn-off stars from the halo star sample, we plot the data in the $B-V$ vs. absolute magnitude B diagram, which is equivalent to the H-R diagram, overplotted with GARSTEC isochrones (the Garching Stellar Evolution Code, Weiss & Schlattl 2008) (Fig. 2). The absolute magnitude in B is obtained from their parallax and apparent magnitude in B by using the equation

$$M_B = m_B - \log_{10}(1/\pi) + 5, \quad (7)$$

where m_B is apparent magnitude for the B band, M_B the absolute magnitude for the B band, and π the parallax in arcsec. Although several types of stars can be identified from Figure 2, we only concentrate on the turn-off stars. We define a rectangular region indicated with the magenta box in Figure 2 to select the turn-off stars. The rectangular region covers all the minimum values of $B-V$ for the GARSTEC evolution tracks at Z = 0.0001, 0.001 and 0.004 within tolerance defined by measurement error, which is 0.05 mag and 0.1 mag in color index and absolute magnitude, respectively. Most of the turn-off stars, including the halo turn-off stars, are included in this region with very few contaminations. Finally, 74 sources are selected from the box after excluding 30 binary stars according to SIMBAD.

Even for stars located very close to the Sun, interstellar extinction can still slightly redden the color index and introduce systematic bias into the determination of age. Because all the turn-off stars selected in this work are located within a few hundred parsecs, a 3-D extinction map should be used rather than the total extinction correction based on either Schlegel et al. (1998) or Schlafly & Finkbeiner (2011), which are likely to overestimate the extinction for such nearby stars. Bailer-Jones (2011) introduced a Bayesian method to estimate the intrinsic parameters of $\sim$ 47 000 F, G, K *Hipparcos* stars as well as their extinction with an accuracy of 0.2 mag. For each halo turn-off star in our sample, its extinction is determined by averaging over the stars, which are located within the 2-degree-radius circle and 50 pc in distance around it, from the Bailer-Jones catalog. We do not find any stars located within the 2-degree circle in the Bailer-Jones catalog for nine of the 74 selected halo turn-off stars. Then we adopt the extinction estimated from Schlafly & Finkbeiner (2011) for these nine sources. However, three of them have too large of extinction to be realistic, so we remove them from our sample and leave 71 sources for the age determination.

2.4 Blue Straggler Contamination

According to Xin et al. (2007), the study of the properties of unresolved stellar populations using the evolutionary population synthesis technique should take the contributions of blue stragglers into account. Their study suggests that the contamination of blue straggler stars in the main sequence turn-off sample selected from Galactic open clusters is about 10%. We assume the same contamination rate and remove the bluest eight sources (black dots in Fig. 3), which are much bluer than other sources and are likely to be blue stragglers. Indeed, compared with the isochrones, these eight stars are located in the region that is significantly bluer than the oldest isochrone. This is obviously unrealistic, and even the error bars cannot explain why they are so blue. The remaining 63 stars, marked as magenta points in Figure 3 are finally used to determine the age.

3 THE AGE OF THE HALO

When using isochrones to determine the age of a normal star or white dwarf, one is always confronted with the issue of atomic diffusion, which is the effect of the gravitational settling of heavy elements (Salaris et al. 2000). Due to this gravitational settling, the heavy elements in the

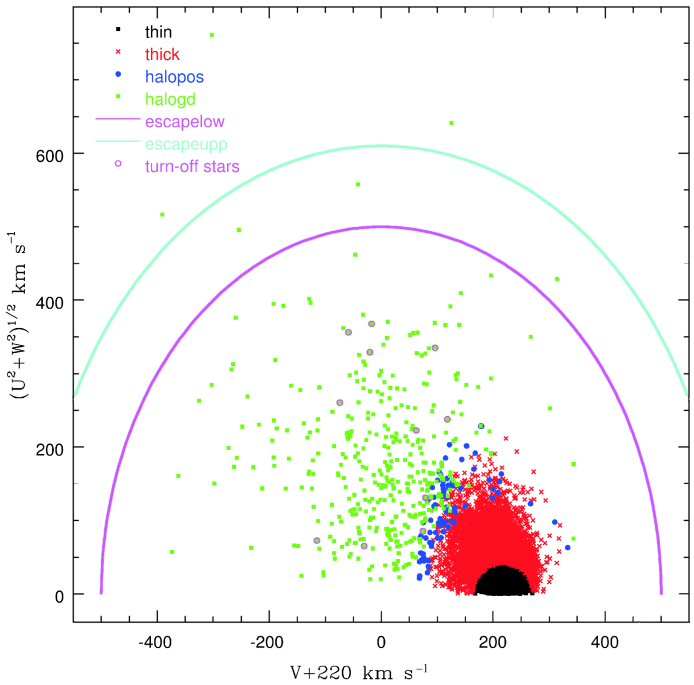

Fig. 1 Selected thin disk, thick disk, possible halo and good halo candidates are plotted in the V+220 km s^{-1} vs. $(U^2+W^2)^{1/2}$ km s^{-1} plane. Almost all stars are well distributed under the lower limit of the escape velocity of Milky Way as we expect, except that a few of them are above the limit or even beyond the upper limit. After further inspection we find three of them are binaries while the others are high-proper motion stars. Pink circles indicate turn-off stars located between 10 Gyr and 12 Gyr isochrones in Figure 3.

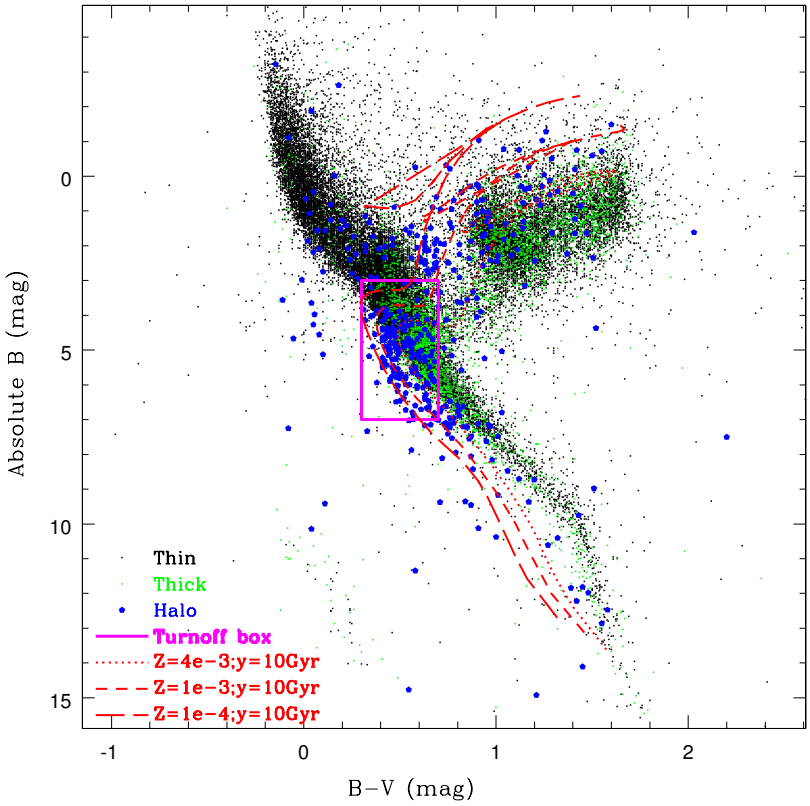

Fig. 2 $B-V$ vs. absolute magnitude B plot for the good halo star candidates overplotted with GARSTEC evolution tracks at $Z=$ 0.0001, 0.001, and 0.004. The black, green, and blue points represent stars from the thin disk, thick disk, and halo respectively. The halo stars within the magenta box are considered to be halo turn-off stars.

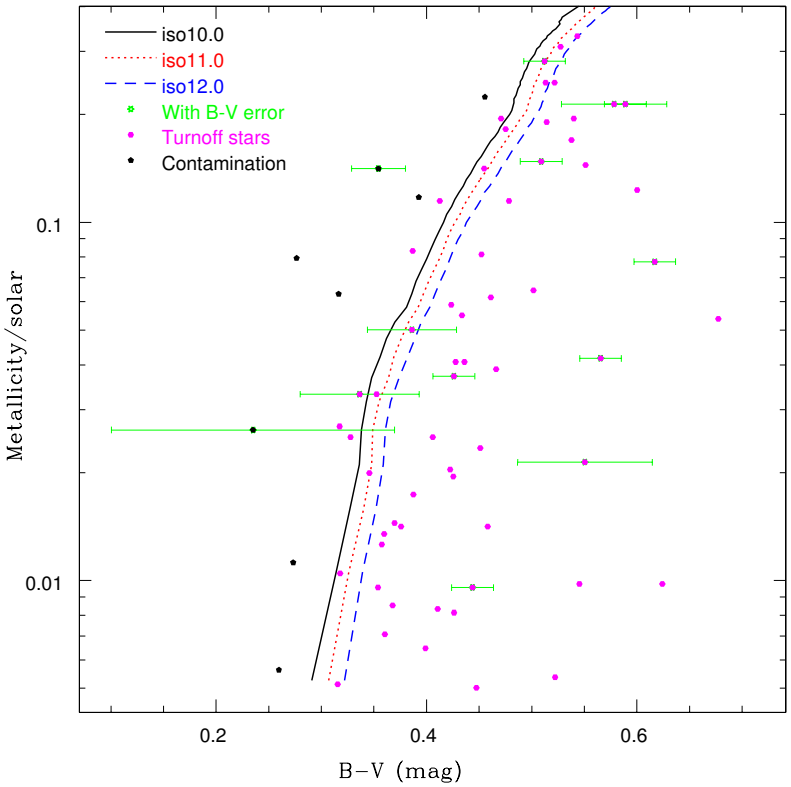

Fig. 3 $B-V$ vs. metallicity/solar plot. The selected turn-off stars are overplotted with the GARSTEC isochrones at 10 Gyr, 11 Gyr, and 12 Gyr. Green bars are the $B-V$ errors. Pink points are the halo turn-off stars, while black points represent the blue straggler contamination.

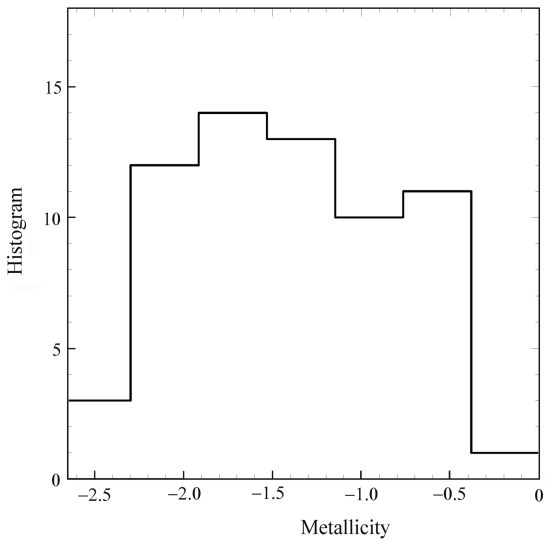

Fig. 4 Distribution of metallicity from turn-off halo stars plotted as pink points in Fig. 3. Even though from this plot, there may be some contamination from the thick disk that exists in the sample of turn-off stars, it does not affect our result much based on our test of removing stars which have metallicity greater than -1.

surface of a star will sink underneath the convective envelope. Meanwhile, a certain amount of hydrogen will move from the center towards the surface. Then, there is less hydrogen left to be burned in the core, thus, the lifetime of the star in the main sequence stage becomes shorter. This process consequently decreases the content of heavy elements during the main sequence stage. It may significantly affect old metal-poor stars, owing to their thin convective envelopes and longer diffusion time. Without considering the effect of atomic diffusion, the age obtained from isochrones can be significantly biased from reality (Bergbusch & Vandenberg 1992; Schuster et al. 1996;

Unavane et al. 1996; Green et al. 1987), and may even conflict with the age of the universe, 13.7 ± 0.2 Gyr (Bennett et al. 2003). Therefore, we use GARSTEC with atomic diffusion in the determination of the age.

In principle, the bluest $B-V$ of a turn-off star is related with both age of the population and metallicity. Therefore, we plot the turn-off stars in the $B-V$ versus metallicity (Z) plane overplotted with GARSTEC isochrones of 10 Gyr, 11 Gyr and 12 Gyr, as shown in Figure 3. The age of the halo in this plane is determined by the position of the blue boundary of $B-V$ for the turn-off stars. Because we only have 63 halo turn-off stars, the blue boundary is not easy to identify by eye. Therefore, we develop a quantitative approach to accurately determine the boundary. It is noted that the separation in $B-V$ between different isochrones is roughly invariant with metallicity. Hence, we define the $B-V$ distance as the distance between a turn-off star and an isochrone with the same metallicity. The best determined age of the halo is then written as

$$\min_{\rm dis} |\Delta_{B-V}(Z|{\rm Age})|, \tag{8}$$

where $\Delta_{B-V}(Z|{\rm Age})$ refers to the distance between the $B-V$ boundary of turn-off stars and the isochrone with Age at metallicity Z. The minimum distance with a certain isochrone corresponds to the best determined age.

In practice, the best determined age of the halo is affected by the uncertainty of $B-V$ and other contaminations in the halo turn-off stars. Thus, the boundary of $B-V$ does not look like a hard boundary but rather is softened and blurred. In order to better determine the position of the blue boundary, we empirically fit the distribution of $B-V$ distance with a given Age using a Gauss-Hermite (G-H) function

$$\begin{aligned} f(x) \;=\; & \frac{1}{\sqrt{2\pi}\sigma} e^{-\frac{(x-\mu)^2}{2\sigma^2}} \Big[1 + \frac{h_3}{\sqrt{3}}(2x^3 - 3x) \\ & + \frac{h_4}{2\sqrt{6}}(4x^4 - 12x^2 + 3)\Big], \end{aligned} \tag{9}$$

where x stands for $B-V$ distance for all Z and a given Age, σ is the standard deviation of the G-H function, μ is the mean, and h_3 and h_4 are the coefficients of the 3rd and 4th order Hermite polynomials respectively. The advantage of using the G-H function is that its derivative can be analytically derived. Also, we select the x at the maximum peak of the derivative of the G-H function as the boundary of $B-V$ distance.

A Monte Carlo simulation is conducted in order to determine the age of the halo taking into account the uncertainty of the photometry. Only 14 stars in our sample have $B-V$ errors and their median value is 0.02 mag. We assume that the error of $B-V$ follows a Gaussian distribution with 0.02 mag as the standard deviation. We then only use isochrones at fixed ages of 10, 10.5, 11, 11.5, and 12 Gyr. For each isochrone, we randomly add errors drawn from the Gaussian distribution to the 63 turn-off stars. Then we derive the minimum of the $B-V$ distance from the maximum peak of the derivative of the best fit Equation (9). Figure 5 illustrates this procedure for one simulation. We repeat a hundred runs of the simulation for each isochrone and obtain the averaged value and the standard deviation of the minimum boundary of $B-V$ distance from the simulated data.

Finally, when the averaged boundaries for all isochrones are measured, the age of the isochrone with the smallest $B-V$ distance at the boundary corresponds to the age of the halo. The isochrone corresponding to 10.5 Gyr is found to be the one with the smallest $B-V$ distance. Moreover, the distribution of the boundary of $B-V$ after 100 simulations can be fitted by a Gaussian profile (Fig. 6). The standard deviation of the distribution corresponding to the isochrone of 10.5 Gyr is 0.023 mag. Considering that the median $B-V$ difference between 10 Gyr and 12 Gyr is about 0.03 mag, the dispersion of the age is consequently obtained as 1.5 Gyr, which is rescaled from 0.023 mag. Therefore, the final age of the halo measured from the field turn-off stars is 10.5 ± 1.5 Gyr.

4 DISCUSSION AND CONCLUSIONS

We estimated the age of the Galactic halo with kinematically selected field halo turn-off stars by comparing their color and metallicity with isochrones. Jofré & Weiss (2011) also used a similar method to determine the halo age with isochrones, but their halo membership is determined using metallicity instead of kinematics. The reason is that the stars they used are from SDSS, in which the distances to the stars are not sufficiently accurate for halo membership identification. Unlike Jofré & Weiss (2011), we only selected the stars with accurate parallax measurement from SIMBAD, whose parallaxes are mainly measured from *Hipparcos*. On the other hand, the age estimation in Jofré & Weiss (2011) is based on temperature and metallicity. The temperature is derived from the spectral fitting with synthetic spectra from atmosphere models, which is somewhat model dependent. We determined the age based on $B-V$ color and metallicity. The apparent magnitudes are from photometric measurement which are essentially accurate. However, the accuracy of the age estimation is limited by extinction correction. Despite the different methods and data we used independently, our estimated age of 10.5 ± 1.5 Gyr is consistent with their result, which is 10–12 Gyr. More recently, Kalirai (2012) estimated the age of the halo using white dwarfs and obtained 11.4 ± 0.7 Gyr. Our result is also in agreement with it.

It can be noted that the uncertainty of our result is quite large compared with other works. It is necessary to analyze the reasons for this uncertainty. First, the sample size used in this work is too small. We finally use only about 60 turn-off stars in the age determination. It is expected that the uncertainty can be significantly reduced if the sample size is enlarged by a few times. Second, the uncertainty of the photometry is slightly large due to the rough extinction correction. Third, the contaminations in turn-off stars include binaries, blue stragglers, pulsators, etc. These contaminations may blur the boundary of the turn-off stars.

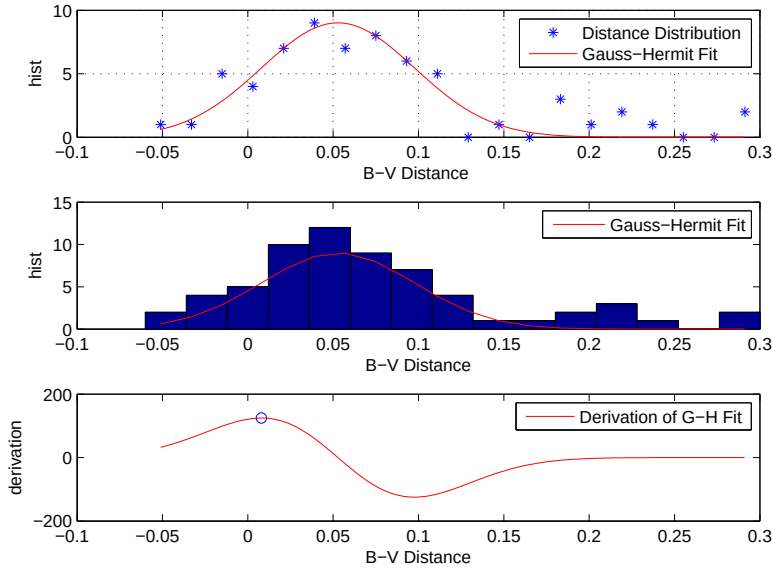

Fig. 5 Illustration of one Monte Carlo simulation for an isochrone at 10.5 Gyr. $B-V$ distance represents the distance between the star and the isochrone. The top and middle panels show distance distribution and G-H fit of the distribution respectively. The bottom panel shows the derivative curve of the best fit G-H profile. The blue circle represents the maximum value of the derivative, which indicates the boundary of the turn-off stars.

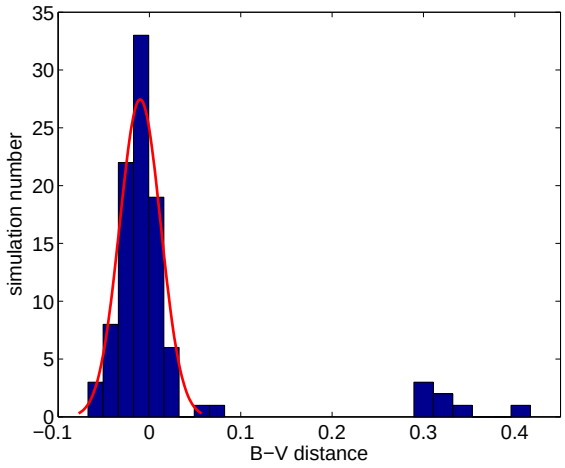

Fig. 6 Distribution of the boundary of $B-V$ distance to the isochrone for 10.5 Gyr after 100 simulations. The red curve is the normal fit for the distribution. The standard deviation (0.023 mag) of this normal fit is adopted as the error of the age. In order to obtain a robust error, a small number of random bad simulations (defined as outliers >0.2) are removed before fitting the distribution.

For instance, the binaries can slightly alter the color index by combining the light from both companions or due to the faster rotation of the primary stars. In addition, blue stragglers are believed to be binary systems with mass transfer. Hence, their luminosity and color index are broadly dispersed and heavily overlap the main sequence stars (Lu et al. 2010). Fourth, according to Figure 4, the majority of our sample belongs to the inner halo. However, the formation of the inner halo is still unclear. Thus, the possible existence of a sub-halo with a different origin, i.e. it fell into the inner halo via disruption and has a significantly younger age, may indicate an intrinsic dispersion of age, which could mix the boundary as well. In the future, we may significantly improve the estimation of age with around a few thousand kinematically identified halo-like turn-off stars from both the LAMOST survey (Deng et al. 2012) and *Gaia* survey (Perryman et al. 2001).

In this paper we derive the age of the Milky Way halo using the selected field turn-off stars. With only 63 halo turn-off stars, we are able to determine the age of the halo with reasonable uncertainty. Atomic diffusion is taken into account by using the GARSTEC model as the evolutionary

tracks and isochrones. This allows us to well match the observed data and the theoretical stellar models to avoid systematic bias in the age determination. The derived age and its uncertainty have also taken into account the errors of photometry and the contribution of interstellar reddening. Finally, the age is constrained to be 10.5 ± 1.5 Gyr. This result is in agreement with previous works, e.g. Salaris & Weiss (2002), Jofré & Weiss (2011) and Kalirai (2012).

Some improvements could be made in the future. For instance, the database we use here is relatively small compared to SDSS (York et al. 2000) and LAMOST (Cui et al. 2012). We plan to use the latest SDSS and LAMOST data, combined with the accurate distance estimates from *Gaia* (Perryman et al. 2001), to further test our method. For the stellar evolution models, we find that the age reduction due to atomic diffusion has to be taken into consideration when trying to determine the age of stars with isochrones. Also, the difference of the derived age with and without considering the atomic diffusion may be as large as 4 Gyr.

Acknowledgements We thank the anonymous referee for constructive suggestions, which improved this paper significantly. We thank professor Achim Weiss for his generous offering of the full version of the GARSTEC stellar evolution model. This work is supported by the Strategic Priority Research Program "The Emergence of Cosmological Structures" of the Chinese Academy of Sciences (Grant No. XDB09000000). JCG and JFL acknowledge the National Natural Science Foundation of China (NSFC, Grant No. 11333004). JCG acknowledges the scholarship awarded by the AMD company. CL acknowledges the NSFC (Grant Nos. 11373032 and 11333003). This research has made use of the SIMBAD database, operated at CDS, Strasbourg, France.

References

Bailer-Jones, C. A. L. 2011, MNRAS, 411, 435
Bennett, C. L., Halpern, M., Hinshaw, G., et al. 2003, ApJS, 148, 1
Bensby, T., Feltzing, S., & Lundström, I. 2003, A&A, 410, 527
Bergbusch, P. A., & Vandenberg, D. A. 1992, ApJS, 81, 163
Carollo, D., Beers, T. C., Lee, Y. S., et al. 2007, Nature, 450, 1020
Chaboyer, B., Demarque, P., & Sarajedini, A. 1996, ApJ, 459, 558
Cui, X.-Q., Zhao, Y.-H., Chu, Y.-Q., et al. 2012, RAA (Research in Astronomy and Astrophysics), 12, 1197
de Jong, J. T. A., Yanny, B., Rix, H.-W., et al. 2010, ApJ, 714, 663
Deng, L.-C., Newberg, H. J., Liu, C., et al. 2012, RAA (Research in Astronomy and Astrophysics), 12, 735
Dotter, A., Sarajedini, A., Anderson, J., et al. 2010, ApJ, 708, 698
Eggen, O. J., Lynden-Bell, D., & Sandage, A. R. 1962, ApJ, 136, 748
Frebel, A., Christlieb, N., Norris, J. E., et al. 2007, ApJ, 660, L117
Green, E. M., Demarque, P., & King, C. R. 1987, The Revised Yale Isochrones and Luminosity Functions (New Haven: Yale Observatory)
Holmberg, J., Nordström, B., & Andersen, J. 2009, A&A, 501, 941
Jofré, P., & Weiss, A. 2011, A&A, 533, A59
Johnson, D. R. H., & Soderblom, D. R. 1987, AJ, 93, 864
Kalirai, J. S. 2012, Nature, 486, 90
Lu, P., Deng, L. C., & Zhang, X. B. 2010, MNRAS, 409, 1013
Perryman, M. A. C., Lindegren, L., Kovalevsky, J., et al. 1997, A&A, 323, L49
Perryman, M. A. C., de Boer, K. S., Gilmore, G., et al. 2001, A&A, 369, 339
Salaris, M., Groenewegen, M. A. T., & Weiss, A. 2000, A&A, 355, 299
Salaris, M., & Weiss, A. 2002, A&A, 388, 492
Sarajedini, A. 1997, AJ, 113, 682
Sarajedini, A., & Demarque, P. 1990, ApJ, 365, 219
Schlafly, E. F., & Finkbeiner, D. P. 2011, ApJ, 737, 103
Schlegel, D. J., Finkbeiner, D. P., & Davis, M. 1998, ApJ, 500, 525
Schönrich, R., Binney, J., & Dehnen, W. 2010, MNRAS, 403, 1829
Schönrich, R., Asplund, M., & Casagrande, L. 2011, MNRAS, 415, 3807
Schönrich, R., Asplund, M., & Casagrande, L. 2014, ApJ, 786, 7
Schuster, W. J., Nissen, P. E., Parrao, L., Beers, T. C., & Overgaard, L. P. 1996, A&AS, 117, 317
Searle, L., & Zinn, R. 1978, ApJ, 225, 357
Unavane, M., Wyse, R. F. G., & Gilmore, G. 1996, MNRAS, 278, 727
Vandenberg, D. A., Bolte, M., & Stetson, P. B. 1990, AJ, 100, 445
Weiss, A., & Schlattl, H. 2008, Ap&SS, 316, 99
Wenger, M., Ochsenbein, F., Egret, D., et al. 2000, A&AS, 143, 9
Xin, Y., Deng, L., & Han, Z. W. 2007, ApJ, 660, 319
York, D. G., Adelman, J., Anderson, Jr., J. E., et al. 2000, AJ, 120, 1579